MEASURING THE ANGLE OF ATTACK – PRACTICAL CONSIDERATIONS FOR THE DEVELOPMENT OF FAULT DETECTION RESIDUALS

Christian Raab[1] & Nicolas Fezans[1]

[1]DLR (German Aerospace Center) - Institute for Flight Systems, Lilienthalplatz 7 - D-38108 Braunschweig, Germany

Abstract

Flight control systems depend on precise and reliable measurements of inertial and air data, which are crucial for maintaining flight safety. Air data sensors, which are exposed to harsh conditions and potential damage, are prone to common cause failures, which increases the risk of errors. Angle of attack (AOA) is particularly critical, as it impacts control laws and autopilot systems. Conventional fault detection via hardware redundancy is inadequate in cases of common cause or sequential sensor failures. Analytical redundancy methods, which integrate diverse sensor data and physical models, can potentially offer a solution. Fault detection residuals, which are computed using independent sensor signals or kinematic relationships, are central to this approach. However, false positives can occur under specific conditions. This paper focuses on angle of attack measurement and the way to check their values and trends using analytical redundancy. Various residual calculation methods are explored, with real flight data from the DLR research aircraft A320 ATRA utilized for validation. This paper analyzes the characteristics of various residuals in the selected maneuvers and conditions. It also provides practical recommendations for utilizing residuals in flight systems and discusses them.

Keywords: Air Data, Fault Detection, Residuals, Flight Safety, Angle of Attack, Flight Mechanics

Nomenclature

Abbreviations

ADR	=	Air Data Reference
ATRA	=	Advanced Technology Research Aircraft
CG	=	Center of Gravity
DLR	=	Deutsches Zentrum für Luft- und Raumfahrt (German Aerospace Center)
FDI	=	Fault Detection and Isolation
FDR	=	Flight Data Recorder

Symbols

α, β	=	angle of attack, angle of sideslip, rad
a_x, a_y, a_z	=	translational acceleration along the body axis, m/s^2
C_L	=	aerodynamic lift coefficient
D	=	drag force, N
δ_e	=	elevator deflection, rad
F	=	force, N
g	=	Earth' standard gravitational acceleration (g_0 = 9.80665 m/s^2)
γ, μ	=	flight path angle, kinetic bank angle, rad
i_H	=	horizontal stabilizer trim deflection, rad
L	=	lift force, N
l_μ	=	mean aerodynamic chord length, m

m	=	total aircraft mass, kg
Ma	=	Mach number
n_x, n_y, n_z	=	load factor along the the body axis, g
p, q, r	=	roll, pitch and yaw rate, rad/s
$\hat{q}$	=	normalized pitch rate, rad
$\bar{q}$	=	dynamic pressure, Pa
Φ, Θ, Ψ	=	roll, pitch and yaw angle, rad
R	=	fault detection residual
S	=	wing reference area, m^2
T	=	thrust force, N
t	=	time, s
u, v, w	=	velocity components, m/s
V_N, V_E, V_D	=	inertial velocities in north, east and downward geodetic direction, m/s
V_{TAS}	=	true airspeed, m/s
V_{CAS}	=	calibrated airspeed, m/s
x, y, z	=	position coordinates, m

Indices

A	=	aerodynamic velocity
a	=	aerodynamic frame
AOA	=	angle of attack
b	=	body-fixed frame
dyn	=	dynamic
g	=	geodetic frame
IRS	=	inertial reference system
K	=	inertial velocity
k	=	inertial frame
$meas$	=	measured
W	=	wind velocity

1. Introduction

In modern commercial aircraft, the angle of attack measurement is a critical input variable for low speed envelope protections. The sensor data must therefore be accurate and reliable. Failure of a system or incorrect measurements must therefore be detected quickly and reliably. Current fault detection systems are usually based on a voting algorithm. The measured sensor values of a system are compared with the measured values of redundant systems. Air data systems currently in use are designed with triple redundancy. If the reading from one system differs from the other two, that system is identified as faulty. The failure of a single sensor is easily detected using this method. In this case, the readings from the remaining air data systems can be used to safely operate the flight controls and automatic assistance functions. Commercial aircraft are usually traveling on flight paths where the operating parameters like altitude and speed only change very slowly. Once at cruising phase, altitude and speed remain nearly constant over a long period of time. The total failure of a sensor for measuring the speed and angle of attack can still be reliably recognized by comparing it with the two remaining air data systems in this flight range. However, the method fails if two sensors fail simultaneously or one sensor is stuck or freezes during constant cruise flight or even fairly steady flight conditions for which no significant deviation can be noticed at first.

This can occur, for example, due to icing of one or more the angle-of-attack vanes. An incorrect measurement can remain unrecognized over a long section of the flight. Starting from a stuck or frozen AOA sensor, if a maneuver leading to a change to the flight parameters (altitude, speed) is performed, the unreliable sensor information can effectively have disabled the envelope protection and remain undetected. If for some reasons, the aircraft and its crew approach the maximum angle of attack, the situation could escalate and result in an unsafe flight situation. Air data sensors are

usually heated so freezing should not occur, but pilot may forget to activate the probe heating, extreme freezing conditions, and maintenance errors can also occur (e.g., during washing or painting of the airplane). Overall, aircraft architectures are built in a very safe way and basic principles (e.g., forbidding single point of failures yielding to potentially catastrophic outcome, spatial segregation, etc.) have been shown to be very effective, when followed closely. The necessity of such design principles has unfortunately also been shown by various incidents and accidents (e.g., McDonnell Douglas DC-10, Boeing B737 MAX).

There are currently various approaches in the literature [1–5] for increasing the reliability of fault detection and generating replacement values for the failed sensors. Signal-orientated methods monitor, for example, frequency content and the exceeding of defined limit values for individual sensor signals. Deviations from normal behavior can thus be detected quickly. In a model-based approach, models describing the relationships between sets of sensors / physical parameters are used to monitor the different sensors. The signals from other flight systems, such as accelerations and rotational rates from the inertial platform and control surface parameters, are used as input to these models. The model output is subtracted from the measured sensor signal. The size of the residual calculated in this way is used to assess whether the sensor under consideration has an error. Concerning the angle of attack various approaches can be found in the literature. In this paper we investigate three different methods for calculating a residual to detect errors in the angle of attack measurement. The first one is the inertial angle of attack based on the measurements of the Inertial Reference System (IRS). Another one uses a synthetic angle of attack using an aerodynamic model, total and static pressure measurements, as well as acceleration and gyro rate measurements from the IRS. A third residual calculation method considers the rate of change in the angle of attack and its kinematic relation to other flight parameters.

Figure 1 – The DLR Airbus A320 ATRA.

The presented investigation considers a case in which the angle of attack sensors function properly (no error), but the aircraft is flown rather aggressively, near the border or the flight envelope, or in the presence of wind. In this case, detection algorithms based on the presented residuals should not produce false alarms, which could result in a misinterpretation of the current flight situation. Many of the methods found in the literature are usually tested with synthetically generated data from a flight simulation. Often, some simplified equations are used but these simplifications are not explained and the test cases shown may also not cover all situations (e.g., no wind included, or only constant wind). Consequently, it is sometimes difficult to assess whether the simplifications and underlying assumptions are valid or not. For our study recorded flight data from the DLR research aircraft Airbus A320 ATRA (Advanced Technology Research Aircraft) shown in Fig. 1 was used. The data used for these investigations included not only ordinary point-to-point flights, but also measurement data from flight tests for system identification with highly dynamic flight maneuvers. In this way, the properties and robustness of the calculation methods could be tested with real flight test data. In the presence of dynamic maneuvers but with no sensor faults, the fault-detection algorithm should not generate false alarms. Even if the flight data originate from an Airbus A320, the flight mechanics relationships and considerations presented here are transferable to all aircraft types. For all residual calculation methods, practical case studies are presented and considerations that should be taken into account when applying them to angle of attack fault detection.

2. Fault Detection Residuals

2.1 Conventional Measurement of the Angle of Attack

Sensors for measuring the angle of attack are usually part of the aircraft air data system including sensors for total and static air pressure as well as the total air temperature. The most common way to measure the angle of attack is a vane installed near the aircraft nose below the cockpit. Another method is to use pressure probes measuring the differential pressure between upper and

lower positions on the probe. The angle of attack is defined as the angle between the vertical and longitudinal airspeed components in the body coordinate system:

$$\alpha_A = \operatorname{atan2}\left(w_{A,b}\,,\,u_{A,b}\right). \tag{1}$$

For the considerations of analytical redundancies, it is important to bear in mind the relationship between the aerodynamic airspeed and the inertial speed, described in the following equation:

$$\vec{V}_A = \vec{V}_K - \vec{V}_W \text{ so leading to } \begin{bmatrix} u_A \\ v_A \\ w_A \end{bmatrix}_b = \begin{bmatrix} u_K \\ v_K \\ w_K \end{bmatrix}_b - \begin{bmatrix} u_W \\ v_W \\ w_W \end{bmatrix}_b \text{ in the body frame.} \tag{2}$$

The airspeed components important for the aerodynamic angle of attack are determined by the difference between the inertial and the wind speed. The wind speed components are usually given in the geodetic coordinate system with axes in the north, east and downward direction. For the determination of the airspeed with Eq. (2) the wind speed vector has to be transformed to the aircraft body axis system:

$$V_{W,b} = M_{bg}\, V_{W,g}\ , \tag{3}$$

with M_{bg} being the transformation matrix between the body and local North-East-Down frames:

$$M_{bg} = \begin{bmatrix} \cos(\Theta)\cos(\Psi) & \cos(\Theta)\sin(\Psi) & -\sin(\Theta) \\ \sin(\Phi)\sin(\Theta)\cos(\Psi) - \cos(\Phi)\sin(\Psi) & \sin(\Phi)\sin(\Theta)\sin(\Psi) + \cos(\Phi)\cos(\Psi) & \sin(\Phi)\cos(\Theta) \\ \cos(\Phi)\sin(\Theta)\cos(\Psi) + \sin(\Phi)\sin(\Psi) & \cos(\Phi)\sin(\Theta)\sin(\Psi) - \sin(\Phi)\cos(\Psi) & \cos(\Phi)\cos(\Theta) \end{bmatrix}. \tag{4}$$

2.2 Inertial Angle of Attack and Sideslip Angle

Accelerations and angular rates from the inertial reference system are the primary source for calculating redundant signals for parameters measured by the air data system. Not exposed to external atmospheric conditions, the IRS is very robust and less prone to error. Besides, errors in the IRS would most probably not be consistent or identical, such that they should be comparatively easy to detect. One of the output signals of the IRS are the inertial velocities in the geodetic reference frame V_N, V_E, V_D, which can be used to determine an inertial angle of attack. First the velocity components must be transformed to the body axes using the transformation matrix described in Eq. (4):

$$V_{K,b} = \begin{bmatrix} u_K \\ v_K \\ w_K \end{bmatrix}_b = M_{bg}\, V_{K,g} = M_{bg} \begin{bmatrix} u_K \\ v_K \\ w_K \end{bmatrix}_g = M_{bg} \begin{bmatrix} V_N \\ V_E \\ V_D \end{bmatrix}_g . \tag{5}$$

The inertial angle of attack α_K is then calculated from the longitudinal and vertical velocity components:

$$\alpha_K = \operatorname{atan2}\left(w_{K,b}, u_{K,b}\right). \tag{6}$$

The inertial sideslip angle can be calculated in the same way from the inertial velocity and its lateral component using the following formula:

$$\beta_K = \arcsin\left(\frac{v_{K,b}}{V_K}\right). \tag{7}$$

When comparing the aerodynamic and inertial angles, it must be noted that the inertial values do not include the wind speed components. This difference can be seen in the speed equation, Eq. (2). This leads to a difference between the inertial and aerodynamic angle of attack, which depends on the current wind situation.

Another important aspect when calculating and comparing the angle of attack is the location of the sensors. Especially highly dynamic maneuvers may lead to different results when not taking into account the lever arms between the considered sensors, e.g., between the angle of attack vane

sensor and the location of the IRS. The measured angle of attack has to be corrected for the dynamic angle of attack using the following equation:

$$\alpha_A = \alpha_{meas} - \alpha_{dyn} \approx \alpha_{meas} - \arctan\left(\frac{-q\, x_{AOA,IRS}}{V_{TAS}}\right). \tag{8}$$

In case of the Airbus A320 the distance $x_{AOA,IRS}$ is –1.775 m because the vane is located aft of the IRS. Additional contributions to the dynamic angle of attack caused by the roll and yaw rate are assumed to be small and are neglected in this equation because the lateral distance between the IRS and the vane is small compared to the longitudinal distance. The approximation in Eq. (8) is valid for small α_{dyn} which is the case for the high airspeed and comparatively low absolute pitching rate values flown by the Airbus A320. If the wind is neglected, a residual can be defined by comparing the inertial and aerodynamic angles of attack:

$$R_{\alpha_K} = \alpha_A - \alpha_K. \tag{9}$$

2.3 Synthetic Angle of Attack

The synthetic angle of attack is based on precise knowledge of the aerodynamic lift parameters. The method is explained and examined in more detail in the literature in references [2; 6; 7], and based on estimated parameters of an aerodynamic model. For this purpose, the aircraft forces for the stationary symmetrical straight flight are first considered, as shown in Fig. 2.

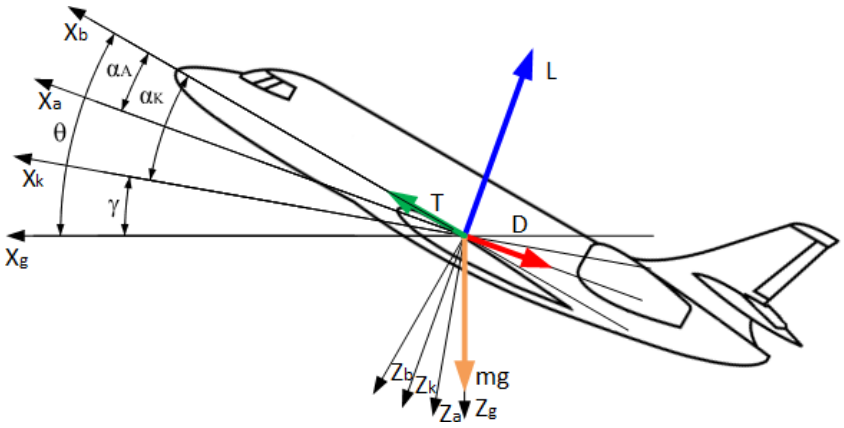

Figure 2 – Longitudinal kinematic forces and different coordinate systems.

The lift force is composed of the forces along the fixed axis system in the x and z directions and can be approximated for small angles of attack ($\alpha_A < 10$ deg) with the following expression:

$$L = F_{x,b}\ \sin(\alpha_A) - F_{z,b}\ \cos(\alpha_A) \approx F_{x,b}\ \alpha_A - F_{z,b}. \tag{10}$$

Using an aerodynamic model the lift force can be expressed as a lift coefficient C_L multiplied by the dynamic pressure $\bar{q}$ and the reference wing area S.

$$L = \bar{q}\ S\ C_L \tag{11}$$

In this case the lift coefficient is modeled with a linear combination of several lift derivatives according to the following expression:

$$C_L = C_{L0} + C_{L\alpha}\,\alpha + C_{L\hat{q}}\,\hat{q} + C_{Li_H}\,i_H + C_{L\delta_e}\,\delta_e + C_{LMa}\,Ma. \tag{12}$$

The IRS measures the accelerations along the body axes, which can be used to calculate the forces $F_{x,b}$ and $F_{z,b}$ respectively. The forces are determined from the load factors according to the following equation:

$$F_{x,b} = m\,a_{x,b} = m\,g\,n_{x,b} \tag{13}$$

$$F_{z,b} = m\,a_{z,b} = m\,g\,n_{z,b}\ . \tag{14}$$

By inserting and rearranging the Eqs. (10–13) the model based angle of attack α_{synth} can be calculated with the following equation:

$$\alpha_{synth} = \frac{\bar{q}\,S\left(C_{L0} + C_{L\hat{q}}\,\frac{q\,l_\mu}{V_A} + C_{Li_H}\,i_H + C_{L\delta_e}\,\delta_e + C_{LMa}\,Ma\right) + m\,g\,n_{z,b}}{m\,g\,n_{x,b} - \bar{q}\,S\,C_{L\alpha}}\,. \tag{15}$$

The accuracy of the estimated values for the synthetic angle of attack is highly dependent on the quality of the aerodynamic model. For the estimation of the aerodynamic derivatives C_{L0}. $C_{L\alpha}$, $C_{L\hat{q}}$, C_{Li_H}, $C_{L\delta_e}$ and C_{LMa} data from a flight test campaign for system identification [8] was used. The derivatives were optimized using a maximum likelihood estimation with the aim that the output of Eq. (15) matches the measured angle of attack from the air data system. This parameter estimation process was repeated for flight data from different aircraft configurations, i.e., flap, slat and gear settings. The total data set included over 360 flight maneuvers in longitudinal and lateral direction. In this way, an angle of attack model was developed that can be used over the entire flight envelope of the Airbus A320 ATRA. The residual which may be used for fault detection is defined as the difference between the measured angle of attack and the synthetic one:

$$R_{\alpha_{synth}} = \alpha_{meas} - \alpha_{synth} \tag{16}$$

2.4 Angle of Attack Rate Residual

Kinematic models, which describe the relationship between flight mechanical quantities, are another way to detect errors in angle of attack measurements. A detailed formulation of the angle of attack rate is often presented in the field of re-entry vehicle guidance and control research [9–11]. In this paper we will examine the time derivative of the angle of attack $\dot{\alpha} = d\alpha/dt$ in more detail and discuss its use as a possible residual for error detection. A very rough approximation of the angle of attack rate would be to use the pitch rate:

$$\dot{\alpha}_A \approx q. \tag{17}$$

However, this approximation neglects the effects of wind and aircraft maneuvering. A more complete approximation, taking into account the roll and yaw rate of the aircraft, would be given by the following equation:

$$\dot{\alpha}_A \approx q - p\cos(\alpha_A)\tan(\beta_A) - r\sin(\alpha_A)\tan(\beta_A). \tag{18}$$

The above approximation does not take into account the effect that the flight path vector of the aircraft may change over time due to maneuvers and therefore a change in the forces in the body z and x direction. These effects can be modeled by adding two additional terms: one for the gravity acceleration and one for the measured accelerations ($a_{z,b}$, $a_{x,b}$) in the considered directions of the body axes at the aircraft CG. If the aircraft is moving in a constant wind field, a possible sideslip angle must also be taken into account in these terms. Considering all effects gives the exact equation for the angle of attack rate:

$$\dot{\alpha}_A = q - p\cos(\alpha_A)\tan(\beta_A) - r\sin(\alpha_A)\tan(\beta_A) + \frac{g\cos(\gamma_A)\cos(\mu_A)}{V_A\cos(\beta_A)} + \frac{a_{z,b}\cos(\alpha_A) - a_{x,b}\sin(\alpha_A)}{V_A\cos(\beta_A)} + \dot{\alpha}_W. \tag{19}$$

The angles γ_A and μ_A are the air-path inclination and bank angle and consider the rotational attitude between the aerodynamic and the geodetic coordinate frames. The last term $\dot{\alpha}_W$ considers a dynamic change in the longitudinal wind velocity components due to a dynamic change of the wind itself, which can usually not be determined properly but often assuming $\dot{\alpha}_W = 0$ will be acceptable. Equation (19) can also be formulated only using inertial quantities for the inertial angle of attack rate:

$$\dot{\alpha}_K = q - p\cos(\alpha_K)\tan(\beta_K) - r\sin(\alpha_K)\tan(\beta_K) + \frac{g\cos(\gamma)\cos(\mu)}{V_K\cos(\beta_K)} + \frac{a_{z,b}\cos(\alpha_K) - a_{x,b}\sin(\alpha_K)}{V_K\cos(\beta_K)}. \tag{20}$$

The inertial angle of attack α_K does not depend on the wind, the term $\dot{\alpha}_W$ is therefore not needed in the kinematic relationship. The kinematic relationship defined in Eqs. (19) and (20) are used frequently in the literature, however it is important to distinguish between aerodynamic and inertial

quantities. Depending on the flight and wind condition a significant difference in the magnitude and trend between the inertial and the aerodynamic angle of attack quantities may exist. For the detection of errors Eq. (19) may be used directly to formulate a angle of attack rate residual:

$$R_{\dot{\alpha}_A} = \dot{\alpha}_A - q + p\cos(\alpha_A)\tan(\beta_A) + r\sin(\alpha_A)\tan(\beta_A) - \frac{g_0\cos(\gamma_A)\cos(\mu_A)}{V_A\cos(\beta_A)} - \frac{a_{z,b}\cos(\alpha_A) - a_{x,b}\sin(\alpha_A)}{V_A\cos(\beta_A)} \tag{21}$$

This residual considers the kinematic relationships between the angle of attack measurement and quantities measured by the IRS. If there are any inconsistencies in the terms described by Eq. (19), the residual will deviate significantly from zero. A dynamic change of the wind longitudinal velocities $\dot{\alpha}_W$ is neglected in this residual formulation. It should be noticed that the term using the the air-path inclination and bank angle can also be rewritten based on Euler angles and the angle of attack:

$$\cos(\gamma_A)\cos(\mu_A) = \cos(\Theta)\cos(\Phi)\cos(\alpha_A) + \sin(\Theta)\sin(\alpha_A) \tag{22}$$

This formulation is considered in the practical application working with flight test data, because the measured pitch and roll as well as the angle of attack are directly available. The α_A being used as derivative in Eq. (21) is the measured angle of attack corrected by the dynamic effects as defined in Eq. (8). However, the the acceleration sensors used as input for the angle of attack rate equation are part of the digital flight data recorder (FDR) and are located in the mid of the aircraft near the CG. In this case the lever arm $x_{AOA,FDR}$ for the calculation of the dynamic angle of attack is 9.863 m.

3. Analysis of Different Flight Maneuver Use Cases

In this section maneuvers representing various flight conditions are presented demonstrating the characteristics and behavior of the fault detection residuals. The maneuvers were selected from several flights performed with the DLR Airbus A320 ATRA. For the analysis of the residuals, the measured values recorded by the aircraft sensors were used and further processed according to the analytical formulas defined in section 2. One of the aims of the study was to ensure that the residual algorithms can be implemented on existing hardware and can be executed under operational conditions. For this reason the algorithms were implement in MATLAB/Simulink as continuous simulation model with a fixed time step of 40 ms.

3.1 3211-Elevator Multistep-Input Excitation

Dynamic flight maneuvers can have a major influence on the residuals of the calculated substitute values for the angle of attack measurement. One maneuver where these effects can be clearly demonstrated is a 3211 multistep input on the elevator. Figures 3 and 4 show the time history of several flight parameters for this maneuver. The example presented here was performed during a system identification campaign. For the purpose of the system identification maneuver, the test was performed with the Airbus A320 in “Direct Law”, which explains the aircraft response to the 3211 multistep elevator input of the pilot. Note, however, the control law used has no impact on the mathematical relationships between sensors used by the residuals on which this paper is focusing. The first plot in Fig. 3 shows the measurements of the calibrated airspeed and Mach number from the ADR1 system. Line plots for the pitch rate (blue) and the vertical load factor (red) are presented in the second plot.The last plot shows time series for the measured angle of attack α_{meas} by the ADR1 system, the angle of attack corrected for the position of the FDR accelerometers α_A and the dynamic angle of attack α_{dyn}. In this case the dynamic angle of attack correction was determined for the location of the FDR as mentioned using Eq. 8 with the corresponding distance between the angle of attack vane and the FDR. With the beginning of the pitch moment excitation it slightly deviates from zero. At around 12 s it reaches a maximum of around 1 deg, being also the minimum of the pitch rate of around 9.8 deg/s. As the maneuver progresses, the amplitudes of the values are repeated with reversed signs. A comparison of the curves of the measured angle of attack and the one corrected for dynamic effects shows that a dynamic pitch maneuver generates differences in the local angle of attack. This difference must be taken into account when comparing angle of attack measurements from different sensor locations and calculating the angle of attack rate residual, where the FDR acceleration sensors and the angle of attack vane have different positions. Figure 4 shows

time history plots of additional flight parameters for the excitation maneuver. The first plot shows measurements for the pitch and roll angle. The second plot shows the measured angle of attack corrected for dynamic effects in blue, the inertial angle of attack in red and the synthetic angle of attack in green. Time series plots for the inertial R_{α_K} and synthetic $R_{\alpha_{synth}}$ angle of attack residuals, as well as for the angle of attack rate residual $R_{\dot{\alpha}}$, are presented in the last chart. The line plots for the different residuals allow the analysis of their characteristics under the considered flight condition. At the beginning of the maneuver the inertial and the synthetic angles of attack show only very small deviations from the measured one.

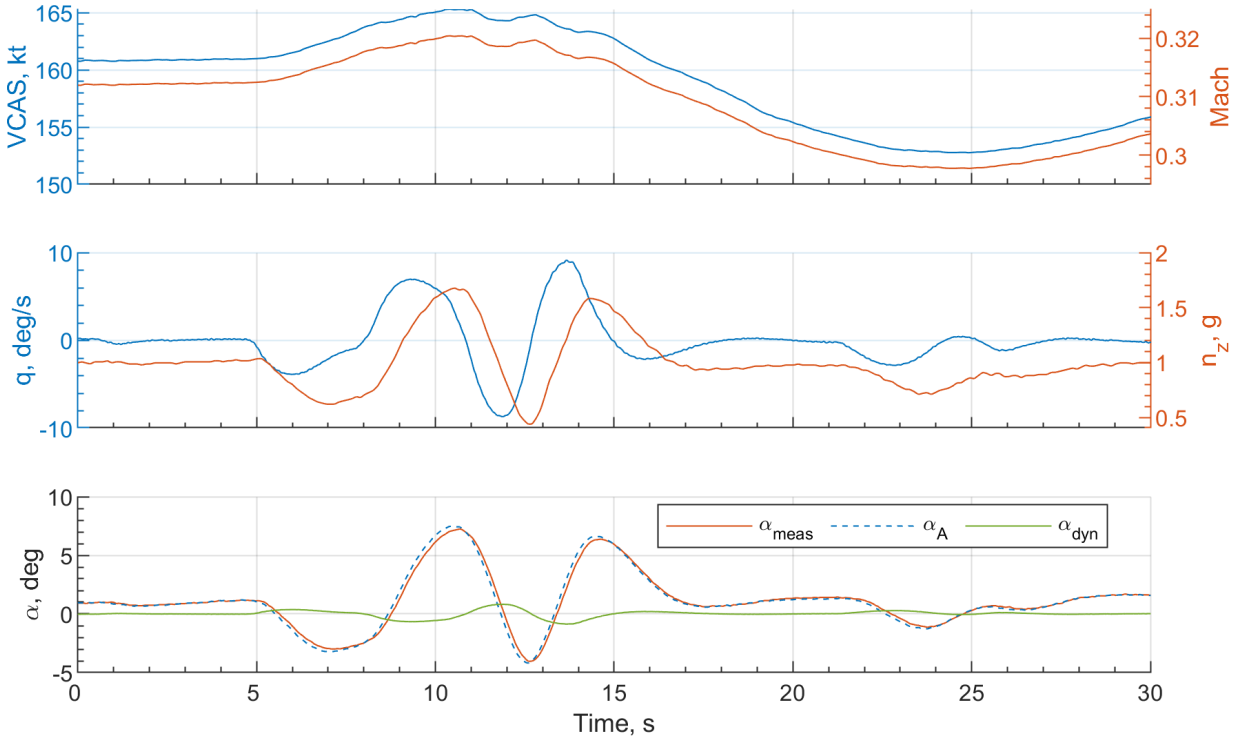

Figure 3 – Dynamic angle of attack effect during a 3211-elevator multistep-input excitation.

This is also indicated by the values for the corresponding residuals. During the pitch maneuver the difference between the inertial angle of attack and the measured one reaches a maximum value of 0.5 and a minimum value of about –1 deg. The deviation is particularly pronounced in the oscillation peaks. This is likely due to low-pass filtering of the sensor measurement in the inertial platform. The residual for the synthetic angle of attack remains fairly stable around a constant value of about 0.3 deg. Only at the minimum of the measured angle of attack the synthetic one shows a peak of about 1.2 deg. Note that as the two types of residuals (bottom plot in Fig. 4) use different y-scales and have different physical dimensions and units, a change in scale could give a complete different visual impression. One reason for that could be the lack of precision of the static linear aerodynamic model which is used for the calculation. Unsteady aerodynamic effects, structural deformations, transport delay in the downwash of the main wing onto the horizontal stabilizer are just a few effects that could play a role in explaining this peak. The angle of attack rate residual $R_{\dot{\alpha}}$ is the only one of these residuals which seems to have no offset with respect to zero. It remains near zero at the start of the maneuver, however during the excitation maneuver it shows a maximum amplitude of nearly ±1 deg/s. Although the amplitude is considerably smaller than the pitch rate q variation, which has an amplitude of nearly ±10 deg/s. One potential reason for the deviation from zero could be the data acquisition process of the different sensor measurements. The accelerations $a_{x,b}$ and $a_{z,b}$ are sampled at a rate of 8 Hz, originating from the FDR system. Although the accelerations measured by the IRS have a higher rate, the signals that are meant to be used by the control laws are low-pass filtered missing higher dynamics and causing a time delay / phase shift. For this reason the measurements from the FDR accelerometers are used in the following. The angle of attack α_{meas} is sampled at a rate of 10 Hz, while the pitch rate q is measured by the IRS at a rate of 50 Hz. Small delays between the different

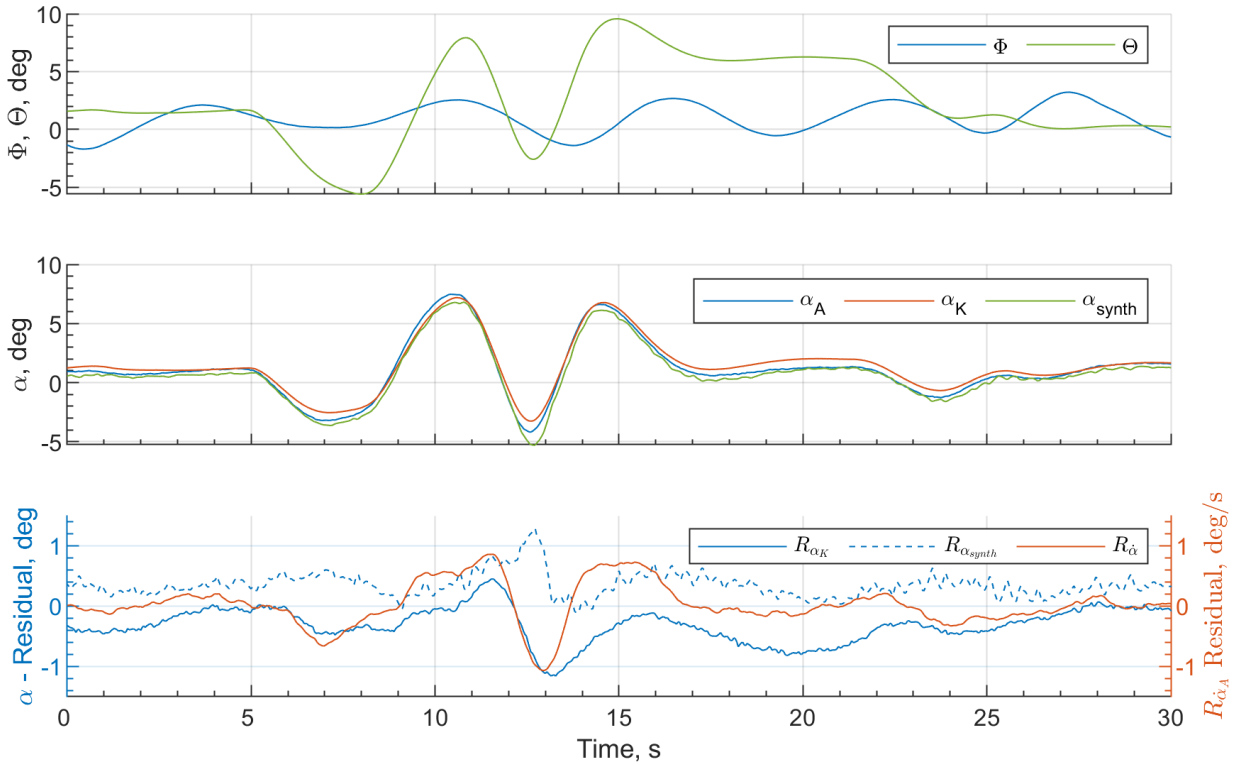

Figure 4 – Analysis of fault detection residuals during a 3211-elevator multistep input maneuver.

signals can cause differences during high dynamic excitation in the residual described by Eq. (19). The error response may also be affected by slight delays or low-pass filters in the measurement chain of one or more of the considered sensors or result from the fuselage bending under load. The first fuselage bending mode frequency is usually about 10 times larger than the main frequency of the pitch excitation: the fuselage will deform with the load factor variation during the maneuver. The effects described must be taken into account when using the residual values for fault detection. In order to prevent false alarms, it is necessary to define a sufficiently large tolerance band for the different residuals. Further investigations are required to optimize signal processing and define the detection thresholds.

3.2 Turn Maneuver in a (Fairly) Constant Wind Field

When considering inertial and aerodynamic parameters, it must be noted that wind speed must not be neglected under certain flight conditions. The example discussed in this section illustrates that the inertial and measured angle of attack and their trends can differ massively, for instance during a turn in a constant wind field. Figure 5 shows the flight data measurement from the Airbus A320 ATRA for such a turn maneuver. The first three charts show the time series plots for the airspeed V_{CAS}, Mach number, rotational rates (p,q,r) and attitude angles (Φ,Θ,Ψ). On the last chart, time history plots for the wind velocity vector components (u_W, v_W, w_W) in the geodetic (indices 'g') and aircraft body (indices 'b') frames are shown. The velocity components were determined in a post-process of the flight data using Eq. (2) and more accurately calibrated angle of attack and sideslip measurements. The wind blows from a north eastern direction and stays nearly constant throughout the turn maneuver. This is indicated by the geodetic velocity components which are approximately 14 kt in the southward and nearly 40 kt in the eastern direction. The downward wind velocity is nearly zero. This leads to a magnitude of the wind velocity V_W of approximately 42 kt. The maneuver starts with a horizontal wings-level flight condition with a nearly constant speed of approximately 237 kt. At 5 s, a constant turn to the left is initiated.

Roll rate and bank angle begin to increase until 12 s, at which point the bank angle remains at –20 deg and the roll rate returns to near zero. Calibrated airspeed and pitch angle remain nearly constant throughout the turn maneuver. Two notable effects can be observed in the flight data for

the turn maneuver. The first effect is the buildup of a constant yaw and pitch rate at the initiation of the turn, which remain constant throughout the turn. Another effect can be seen in the curves for the wind speed components. While the curves in the geodetic system remain constant, the velocity components for the wind in the longitudinal and vertical directions in the body-fixed system change, because the body frame is not an inertial (Galilean) frame of reference in that case. This illustrates the fact that the trends/slopes of α_K and α_A may significantly differ, even when flying in a nearly perfectly constant wind field. The time histories shown in Fig. 6 allow a detailed analysis of the effects of the turn maneuver on the angle of attack and the calculated residuals. The first chart shows the line plots for the inertial angle of attack (blue), the angle of attack corrected for dynamic effects (red) and the synthetic angle of attack (green).

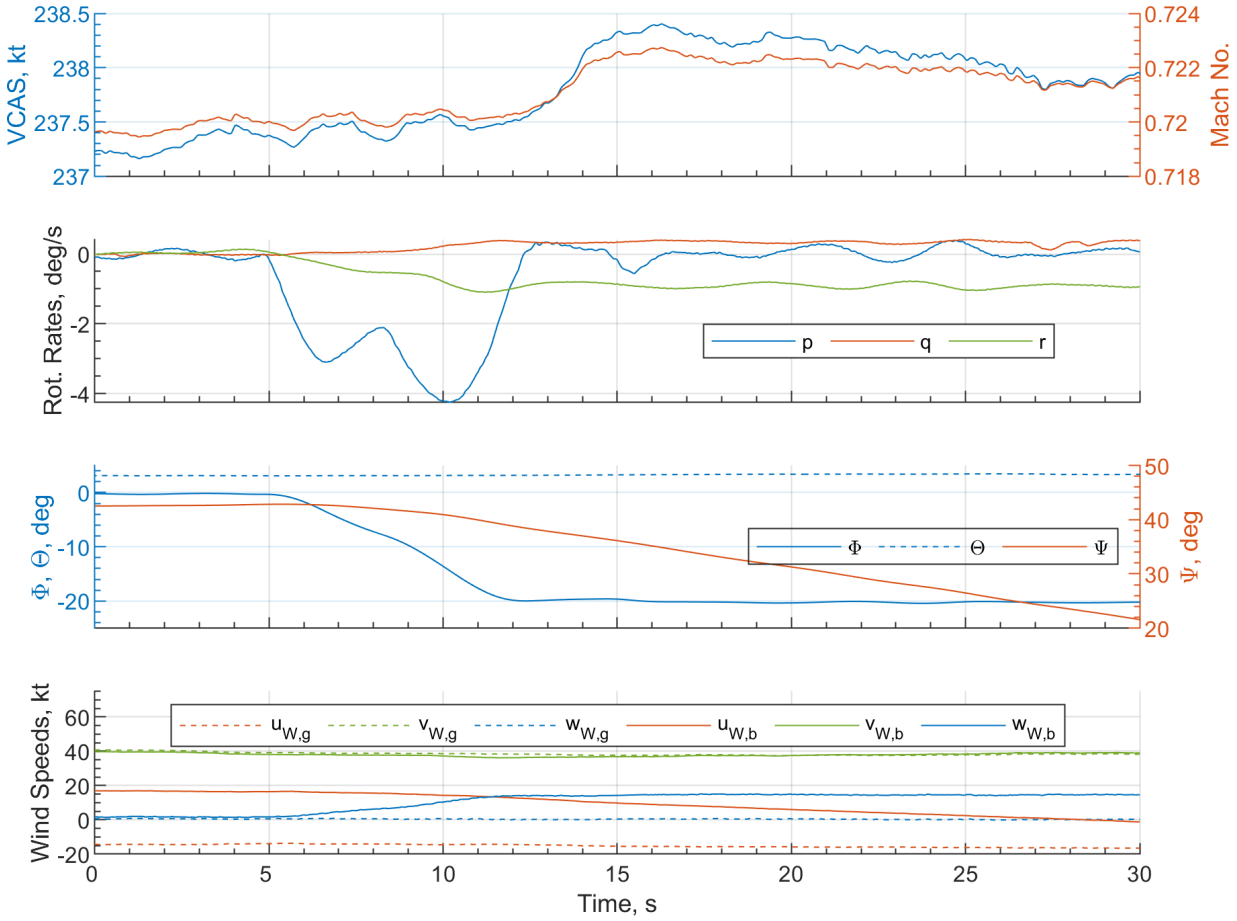

Figure 5 – Flight test parameters during a turn maneuver in a constant wind field.

At the beginning of the maneuver all quantities remain near 3 deg, however at the beginning of the turn maneuver the inertial angle of attack α_K starts to deviate significantly from the measured and the synthetic one. During the turn maneuver it stays at about 5.2 deg, whereas the other ones show also a small increase to 3.4 deg, but have almost the same value. This characteristic is also visible in the line plots for the residuals presented in the third diagram of Fig. 6. $R_{\alpha_{synth}}$ remains near zero during the maneuver, whereas R_{α_K} increases up to less than –2 deg. One reason for this deviation is the stationary wind field through which the aircraft moves during the turn maneuver. The plot for the wind speeds in the geodetic system shows that the components of the wind speed vector are almost constant.

Another way to look at the same relationship starts with considering again Eq. (2). This equation results directly from the definition of the coordinate systems and basic kinematics, so that it always perfectly holds. And as already mentioned, the components of the wind speed in the body-fixed system change with the initiation of the turn (the wind vector projection onto the the vehicle body axes change with its orientation). However, the aerodynamic airspeed vector in the body frame

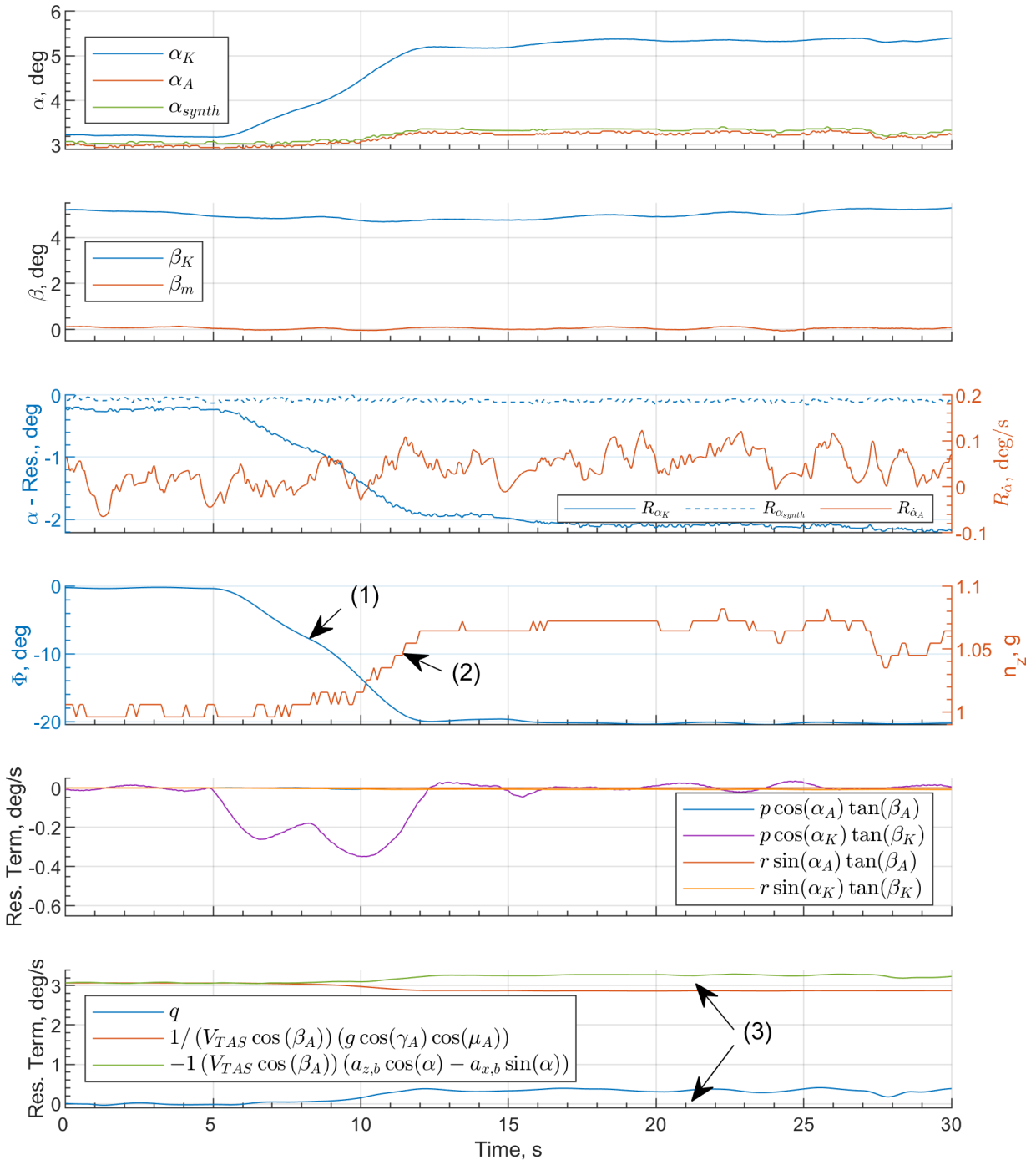

Figure 6 – Flight parameters and single residual terms during turn maneuver in a constant wind field.

remains almost constant (minimum increase of α_A to increase the load factor n_z). This means that the inertial airspeed vector components in the body frame must change to compensate the variation of the wind vector body frame components. For this reason the inertial angle of attack deviates from the measured one during the turn maneuver.

A third way to conceptualize this effect, is to say that we had an horizontal wind, causing a drift that was contained in the horizontal plane, but that with the tilting of the z_b axis, it now has a noticeable component in this direction. The residual R_{α_K} for and the α_K (and its trend) can hardly be useful for air data monitoring without properly accounting for this effect. Unfortunately, such effects seem too often to be overlooked due to approximated equations or too simple test scenarios/simulation models. The case that was shown is far from being extreme and airliners often encounter even worse situations with wind shears or during the buildup/downburst of a thunderstorm. These situations may threaten the safety of the flight, if not properly handled by the crew, so having false alarms generated in such

conditions is even less desirable than under normal flight conditions.

Another discrepancy between inertial and aerodynamic quantities is depicted in the second plot of Fig. 6. Here, line plots for the inertial (blue) and the aerodynamic sideslip angle (red) are presented. In this case, the inertial sideslip angle was determined by Eq. (7), whereas the aerodynamic one was measured by a separate wind vane installed below the aircraft radome. The aerodynamic sideslip angle remains near zero throughout the entirety of the turn maneuver, resulting from the turn coordination function of the flight control system. In contrast, the inertial sideslip angle commences at nearly 5 deg and only exhibits slight decreases during the maneuver. This discrepancy between inertial and aerodynamic sideslip is again attributed to the wind field in which the aircraft is moving and correspond roughly to the drift angle (if $\gamma \neq 0$, the (x_k, y_k) and (x_a, y_a) planes are not perfectly horizontal). In the considered time slice, the changes in the inertial sideslip angle are relatively minor, as the heading change is only from 45 to 20 deg. On a complete turn, it would have changed sign and behaved approximately like a sine wave.

The reason for the small increment of the measured angle of attack α_A can be explained with line plots in the fourth plot, where the progression of the bank angle Φ and the vertical load factor n_z are presented. As the bank angle starts to increase to –20 deg, indicated by point No. 1, the vertical load factor increases from 1 to 1.05 g and stays constant during the turn as indicated by point No. 2. This additional vertical force is intentionally commanded by the normal law to compensate for the turn (note that $\forall t, |\Phi(t)| \leq 33\,\text{deg}$) and maintain a constant altitude (or flight path angle) during the turn. For this reason the aerodynamic angle of attack is increased slightly as part of the maneuver: this increase is very small compared to the α_K variation.

The angle of attack rate residual, $R_{\dot{\alpha}}$, appears to be largely unaffected by the turn maneuver in the wind field, fluctuating around zero with a minimum amplitude of –0.08 deg/s and a maximum amplitude of 0.15 deg/s. Upon examination of the individual terms of the angle of attack rate equations, it becomes evident that a strong simplification or mixed use of inertial and aerodynamic terms of this equation is only acceptable under certain conditions. The fifth plot in Fig. 6 displays line plots for terms of Eqs. (20) and (19) as they are affected by the aircraft yaw and roll rate. While the line plots for the other terms remain near zero, the one for the term "$p\cos(\alpha_K)\tan(\beta_K)$" in violet deviates from zero during the initiation of the turn, reaching a minimum of nearly –0.38 deg/s. This term returns to zero with the aircraft reaching a stationary turn condition. This behavior can be attributed to the roll rate at turn initiation and an existing inertial slip/crab angle caused by the wind. This characteristic of the inertial angle of attack rate is in accordance with the change of the inertial angle of attack depicted in the first plot of Fig. 6. The final chart presents line plots for the remaining terms of the aerodynamic angle of attack rate equation (cf. Eq. (19)). The orange line depicts the angle of attack rate resulting from a change in the aircraft's gravity vector. This can be thought of as the tendency of the flight path vector of a free falling object to go down to –90 deg and to move towards the object that attracts it (in this case the Earth). The green line represents the opposite of the angle of attack rate caused by body accelerations in the vertical and longitudinal directions. This can be thought of a the tendency of the flight path vector, and so the trajectory, to be bend by the aerodynamic lift force. In steady flight both gravity and lift force are perfectly opposite to each other and so is the green line on top of the orange one during the first 5 s of the plot, before the maneuver starts. Again, to ease the visual comparison of these two terms, the last one has been multiplied by -1.

The pitch rate indicated by the blue line plot is small compared to the other terms. Consequently, the angle of attack rate remains near zero. At 5 s, the turn is initiated, resulting in a change of the bank angle to –20 deg, indicated by point No. 1. This causes a reduction of the term responsible for the change of the gravity vector (due to the cosine of μ_A). Similarly, as marked by point No. 2, the vertical load factor has increased. Therefore, the line plot for the term containing the vertical acceleration in the body frame has also increased. A relatively constant difference is observed between angle of attack rate equation terms corresponding to the gravitational acceleration and the acceleration in the body coordinate system, represented by the orange and green line plots, cf. point marked with the No. 3. However, since the aerodynamic angle of attack remains constant (to a slightly increased value but constant) during the turn maneuver, the resulting difference between the two terms must be

compensated. This is achieved by a constant pitch rate q, as indicated by the blue line plot. Note that it has approximately the same value as the difference between the two terms marked by point No. 3. The acceleration during the turn means that the flight path vector (with respect to the surrounding air mass) is moving in the horizontal plane: part of this rotation rate is aligned with the body y axis and the pitching rate q simply corresponds to the body frame rotation that compensate with change in flight path vector direction and thereby ensures that the flight path vector remains constant in the body frame.

The examination of the individual components of the angle of attack rate equations illustrates that external factors such as wind and maneuvers that deviate from a level flight trajectory can influence the angle of attack rate due to non-constant flight path vector orientation. In fairly similar sets of equations, this effect is described based on the time derivatives of the flight path angle $\dot{\gamma}$ and of the track angle $\dot{\chi}$ (see for instance [9, Eq. (14)] or [11, Eq. (2.5.2)]). Failure to account for these effects may result in erroneous conclusions when utilizing a simplified angle of attack rate equation as a fault detection residual.

3.3 Deceleration and High Angle of Attack Situation

Some of the potentially dangerous situations that could result from erroneous angle of attack measurements involve nearing or exceeding the stall angle of attack. Various effects are interesting to look more closely on real data. First, when the angle of attack approaches the stall angle of attack value (exact value depends on the slat/flap configuration and Mach number), the flows over the wings starts to detach near the trailing edge of the wing and the separation point moves gradually towards the leading edge with increasing angle of attack. The lift curve progressively flattens and the local slope nears zero and even becomes negative, see [12]. Additional vibrations (low speed buffeting) can occur as well. The small angle approximation used for deriving α_{synth} and leading to the formula of Eq. (15) becomes worse with increasing value of the angle of attack. The error made through this approximation is in the order of a few percents and the deviation of residual $R_{\alpha_{synth}}$ is much larger, so the small angle approximation is not the main source of error.

To illustrate the challenges, for the different residuals and proposed techniques, posed by larger and slow variations of the angle of attack as well as approaching the stall angle of attack, a deceleration maneuver up to the stall protection of the Airbus A320 ATRA is considered. Several time histories of the flight parameters for this maneuver are presented in Fig. 7. The first plot presents measurements for the airspeed VCAS as a blue and the Mach number as a red line plot. The maneuver begins with an airspeed of approximately 133 kt and then proceeds with a deceleration towards 112 kt, after which the aircraft recovers to an airspeed of 138 kt. The second diagram depicts the aircraft attitude angles. During the initial 20 s of the maneuver, there is a minor change in heading to the left, from 14 deg to 5 deg, as indicated by the red line. Concurrently, the bank angle is nearly –5 deg, as shown by the blue line. For the remainder of the maneuver, the aircraft maintains a horizontal flight condition. The pitch angle is indicated by a green line, which begins at 9 deg and increases to nearly 15 deg during the deceleration.

The third plot presents the different wind velocity components in the inertial and body axes. In this case, the wind is nearly constant, with a northern component of 8 kt, an eastern component of –6 kt, and a vertical component near zero. The fourth diagram displays time series for the vertical load factor n_z and pitch rate q. The load factor, indicated by the blue line, exhibits a small peak of 1.12 g at 8 s, which can be attributed to the small heading change at the start of the maneuver. It remains near 1 g during the deceleration phase from 20 to 85 s, indicating a quasi-steady flight situation. At approximately 90 s, the aircraft is recovered, and the vertical load factor reaches a minimum of nearly 0.9 g.

Over a period of over 60 s, during which the aircraft is decelerating while roughly holding n_z to 1 g, the aerodynamic angle of attack is constantly increasing. This characteristic is illustrated in the fifth plot of Fig. 7, where the line plots are presented in blue for the corrected angle of attack, in red for the inertial angle of attack, and in green for the synthetic angle of attack. The aerodynamic angle of attack begins at approximately 9 deg and reaches a maximum of nearly 17.5 deg at the time point of

85 s. Inertial and aerodynamic angles of attack exhibit a similar progression, whereas the synthetic angle of attack does not. At point No. 1, the synthetic angle of attack begins to deviate, exhibiting a lower value than the other angles of attack. The discrepancy reaches its maximum at point No. 2, which coincides with the highest angle of attack.

This phenomenon is also evident in the line plots for the angle of attack residuals presented in the last plot. During the deceleration maneuver, the inertial angle of attack residual R_{α_K} (blue) remains around zero degrees, whereas the synthetic angle of attack residual $R_{\alpha_{synth}}$ slowly increases up to nearly two degrees. The discrepancy can be attributed to the fact that the aerodynamic model, which serves as the foundation for the synthetic angle of attack calculation, is not sufficiently accurate for flight conditions at high angle of attack. The model defined in Eq. (15) incorporates only linear terms for the aerodynamic derivatives.

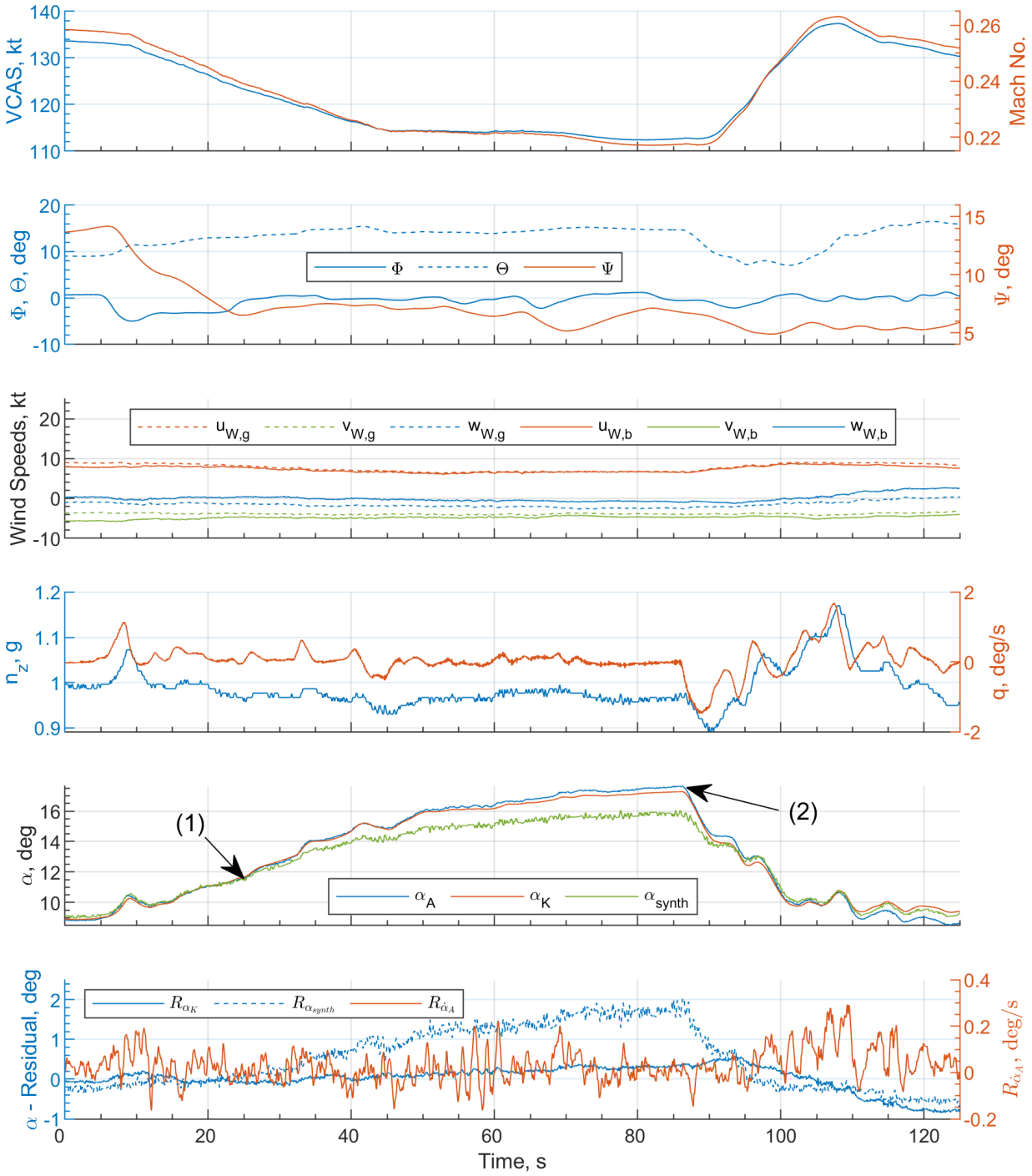

Figure 7 – Flight test parameters and residuals during a high angle of attack maneuver.

However, in regions with a high angle of attack, the lift curve, for instance, exhibits a nonlinear progression, which is neglected in the used lift model. It is therefore evident that it is of critical importance to be aware of the limitations of the aerodynamic model when utilizing the synthetic angle of attack as a control input. Piloting the aircraft in close proximity to stall velocity is not a highly critical flight situation as such, but corresponds to a situation in which margins for errors are reduced. Being in such a state could also already be the result of a temporary loss of situation awareness by the crew. False alarms, potentially inducing (further) confusion, must be avoided at all costs. At the same time, still handling real faults properly remains valuable, so simply disabling fault detection / monitoring functions when approaching stall is not an option either. When employing the residual $R_{\alpha_{synth}}$ to detect errors in the alpha measurement, it is of vital importance to take into account the existing limitations of the aerodynamic model and to test thoroughly the robustness of any monitoring solution based on a lift model near (or even during) stall. The use of the inertial angle of attack residual $R_{\alpha K}$ might also be an fall back option for the detection of faults. In this instance, however, it is necessary to make a prior estimation of the wind speed components in order to assess the residual correctly.

The angle of attack rate residual, $R_{\dot{\alpha}_A}$, is also depicted in the diagram as a red line plot. During the deceleration phase, the residual fluctuates around zero with a maximum deviation of ±0.3 deg/s. The residual is not affected by the presented critical deceleration maneuver and may therefore be a useful parameter for the detection of faults in the angle of attack sensor. This is not surprising at this residual purely relies on kinematic relationships which are not affected by model errors. Further investigations with real or simulated error cases are necessary to determine the usefulness of this residual more precisely.

4. Conclusion and Outlook

The angle of attack is a critical parameter for ensuring the safety of flight. Consequently, errors in the measurement shall be identified and isolated in a timely and reliable manner. Two methods for calculating inertial and synthetic substitute values were presented. Three different residuals that can be employed for the detection of faults in the angle of attack were evaluated. The utilization of the substitutes and the corresponding residuals was illustrated and discussed using real flight data from the Airbus A320 ATRA research aircraft from DLR. Flight maneuvers corresponding to different flight conditions and including dynamic pitching maneuvers, turn initiation in the presence of significant wind, and a high angle of attack situation are included. They constitute challenging conditions for which certain corrections must be applied and nonlinear effects must be considered to prevent false fault detections. All cases shown in this paper are from real flights with no fault and so candidate residuals / criteria for fault detection should ideally not react too heavily in these cases. The analysis of the various residuals revealed the following:

- It is important to note that when utilizing the inertial angle of attack, the influence of wind must be taken into account. Even for non extreme weather conditions (e.g. constant horizontal wind), there may be a significant discrepancy between the aerodynamic angle of attack and the inertial angle of attack, for instance, during turn maneuvers. In practice, even more extreme conditions could be encountered (e.g., wind shear, downburst).
- It is essential to properly distinguish between inertial and aerodynamic variables, for example, when determining individual terms in the angle of attack rate residual. Failing to consider this aspect when employing the angle of attack rate residual may result in the generation of false alarms. As a direct consequence, any development and validation of air data sensor fault detection methods/systems should always include significant testing with significantly broad range of wind conditions.
- The angle of attack rate residual only involves terms which are either zero or can be shown to cancel each other out in steady 1 g flight conditions. It therefore requires dynamic excitation in order to function: reasonably small lateral and longitudinal flight maneuvers or some minimum level of turbulence should be sufficient to effectively detect erroneous measurements. As it relies only on kinematic equations (no model error), the threshold level can be set to fairly low values, provided that the measurements included in the calculation of the residual are not

affected by delays, excessive noise, or calibration errors.

- The synthetic angle of attack residual is highly effective in numerous flight scenarios, as it accounts for the wind velocity. However, the accuracy of this approach is highly dependent on the quality of the underlying aerodynamic model. The omission of non-linear terms in regions with high angle of attack or highly dynamic maneuvers may result in the generation of false alarms.
- It seems that the residuals considered have complementary strenghts and weaknesses, such that some combinations of these residuals are likely to provide an effective approach for the detection of angle of attack sensor faults. For instance, during steady horizontal flight conditions, the synthetic angle of attack residual should be monitored, whereas during aircraft maneuvers, the angle of attack rate residual seems more reactive and accurate.

After having investigated the behavior of these criteria in corner cases and their robustness limits, the next step in the investigation of fault detection residuals will be the investigation of their sensitivity, i.e., their reactions to angle of attack sensor faults. This can for instance be done by falsifying the flight data according to the expected fault signature of the considered fault cases (e.g., blocked alpha vane). Another research focus is the optimization of the signal processing of flight data measurements. The ability to implement the algorithms in a real operating environment is the key to their successful practical use. This also includes the specification of adequate residual threshold values, allowing an optimal trade-off between reliable and reactive detection of faults and false alarm rate.

5. Contact Author Email Address

christian.raab@dlr.de

6. Copyright Statement

References

[1] Joseph. E. Zeis. *Angle Of Attack And Sideslip Estimation Using An Intertial Reference Platform*. Master thesis, Air Force Institute of Technology, Wright-Patterson Air Force Base, 1988.

[2] John Valasek, Joshua Harris, Shawn Pruchnicki, Matthew Mccrink, James Gregory, and David G. Sizoo. Derived angle of attack and sideslip angle characterization for general aviation. *Journal Of Guidance, Control, And Dynamics*, 43(6):1039–1055, 2020. ISSN: 0731-5090. doi: 10.2514/1.G004010.

[3] Daniel Ossmann. Enhanced detection and isolation of angle of attack sensor faults. In *AIAA Guidance, Navigation, And Control Conference*, Reston, Virginia, 2016. American Institute of Aeronautics and Astronautics. ISBN: 978-1-62410-389-6. doi: 10.2514/6.2016-1135.

[4] P. Lu, L. van Eykeren, E. van Kampen, C. C. De Visser, and Q. P. Chu. Adaptive three-step kalman filter for air data sensor fault detection and diagnosis. *Journal Of Guidance, Control, And Dynamics*, 39(3):590–604, 2016. ISSN: 0731-5090. doi: 10.2514/1.G001313.

[5] Angelo Lerro, Manuela Battipede, Piero Gili, and Alberto Brandl. Aerodynamic angle estimation: Comparison between numerical results and operative environment data. *CEAS Aeronautical Journal*, 11(1):249–262, 2020. ISSN: 1869-5582. doi: 10.1007/s13272-019-00417-x.

[6] Richard Colgren, Michael Frye, and Wayne Olson. A proposed system architecture for estimation of angle-of-attack and sideslip angle. In *Guidance, Navigation, And Control Conference And Exhibit*, Reston, Virigina, 1999. American Institute of Aeronautics and Astronautics. doi: 10.2514/6.1999-4078.

[7] S. Myschik, M. Heller, F. Holzapfel, and G. Sachs. Low-cost wind measurement system for

small aircraft. In *Aiaa Guidance, Navigation, And Control Conference And Exhibit*, Reston, Virigina, 08162004. American Institute of Aeronautics and Astronautics. ISBN: 978-1-62410-073-4. doi: 10.2514/6.2004-5240.

[8] Christian Raab. Rapid aerodynamic parameter identification on a large transport aircraft. In *AIAA Atmospheric Flight Mechanics Conference (ISSN: 0021-8669)*, Januar 2014. doi: 10.2514/6.2014-0730.

[9] Daniel Kiehn. Stability analysis and flight control design of the winged reusable launch vehicle refex. *CEAS Space Journal*, 13(1):51–64, June 2020. ISSN: 1868-2510. doi: 10.1007/s12567-020-00319-3.

[10] Nicolas Fezans, Daniel Alazard, Nicole Imbert, and Benjamin Carpentier. Robust LPV control design for a RLV during reentry. In *AIAA Guidance, Navigation, And Control Conference*, June 2010. doi: 10.2514/6.2010-8194.

[11] Erwin Mooij. *Aerospace-Plane Flight Dynamics: Analysis Of Guidance And Control Concepts*. PhD thesis, Tu Delft, Jan. 1998. `http://resolver.tudelft.nl/uuid:fa4dd59d-3792-4888-8aa5-bdb3c0d90b15`.

[12] Dietrich Fischenberg. Identification of an unsteady aerodynamic stall model from flight test data. In *20th Atmospheric Flight Mechanics Conference*, Baltimore, MD, USA, 1995. doi: 10.2514/6.1995-3438.